The 18.6-year lunar nodal cycle and surface temperature variability in the northeast Pacific

Stewart M. McKinnell[1] and William R. Crawford[2]

Received 27 April 2006; revised 24 August 2006; accepted 21 September 2006; published 2 February 2007.

[1] The 18.6-year lunar nodal cycle (LNC) is a significant feature of winter (January) air and sea temperatures along the North American west coast over a 400-year period. Yet much of the recent temperature variation can also be explained by wind patterns associated with the PNA teleconnection. At Sitka, Alaska, (57°N) and nearby stations in northern British Columbia, the January PNA index accounts for over 70% of average January air temperatures in lengthy meteorological records. It appears that the LNC signal in January air temperatures in this region is not independent of the PNA, but is a component of it. The Sitka air temperature record, along with SSTs along the British Columbia coast and the PNA index have significant cross-correlations with the LNC that appear at a 2-year lag, LNC leading. The influence of the PNA pattern declines in winter with decreasing latitude but the LNC component does not. It appears as a significant feature of long-term SST variation at Scripps Pier and the California Current System. The LNC also appears over centennial-scales in proxy temperatures along western North America. The linkage of LNC-moderated surface temperatures to processes involving basin-scale teleconnections expands the possibility that the proximate mechanism may be located remotely from its expression in the northeast Pacific. Some of the largest potential sources of a diurnal tidal signal in the atmosphere are located in the western Pacific; the Sea of Okhotsk and the Indonesian archipelago.

Citation: McKinnell, S. M., and W. R. Crawford (2007), The 18.6-year lunar nodal cycle and surface temperature variability in the northeast Pacific, *J. Geophys. Res.*, *112*, C02002, doi:10.1029/2006JC003671.

1. Introduction

[2] Sea surface temperatures (SST) along the coast of British Columbia become unusually warm in some years [*Tully*, 1937; *Tully et al.*, 1960; *Tabata*, 1985]. These years typically coincide with equivalent extremes in weather, biology, and fisheries in the northeastern Pacific [*Royal and Tully*, 1961; *Wooster and Fluharty*, 1985; *Chavez et al.*, 2002; *DFO*, 2005]. In general, these effects are attributed one of three processes, two of which are linked to El Niño-Southern Oscillation (ENSO): (1) a downwelling coastal Kelvin wave of tropical origin that propagates northward along the continental margin from its origin in the warm pool near Ecuador [*Subbotina et al.*, 2001; *Lluch-Cota et al.*, 2001; *Strub and James*, 2002], (2) an atmospheric teleconnection between Southern Oscillation air pressure disturbances in the tropical Pacific and the location and intensity of the Aleutian Low Pressure system [*Emery and Hamilton*, 1985; *Subbotina et al.*, 2001] that enhances poleward advection of heat in the atmosphere and in the sea via the seasonal Davidson Current, and (3) low-frequency variability associated with decadal/basin scale SST patterns [*Mantua et al.*, 1997; *Mantua and Hare*, 2002; *Bond et al.*, 2003]. These mechanisms have yet to be reconciled with the apparent regularity of the bidecadal frequency that appears in many western North American air and SST records [*Chao et al.*, 2000; *Thejll*, 2001]. Our study explores the hypothesis that some temperature anomalies in the northeastern Pacific, even some of those currently attributed to ENSO, were influenced by the 18.6 year lunar nodal cycle (LNC).

[3] The tilt of the Earth's equator relative to the solar ecliptic (the plane defined by the orbit of the Earth around the Sun) is 23.5°, and the lunar orbit is tilted an additional 5°. The two planes defined by the Earth and lunar orbits rotate relative to each other every 18.6 years. If at one time the maximum declination of the moon in the sky during its monthly orbit is 23.5° − 5° = 18.5°, then 9.3 years later this maximum inclination will be 23.5° + 5° = 28.5°. Another 9.3 years later this inclination will be back to 18.5°. Since the strength of the lunar diurnal tide is directly related to this declination of the moon above the Earth's equator, we observe an 18.6-year cycle in the magnitude of the lunar diurnal tide. Semidiurnal tides are also affected, but to a lesser extent [*Doodson and Warburg*, 1941]. For example, amplitudes of the largest diurnal and semidiurnal tidal constituents, K_1 and M_2, oscillate by 13% and 5%, respectively during an 18.6 year cycle. These oscillations are out of phase, so that 2006 and other years separated by 18.6 years coincide with maximum diurnal and minimum

[1]North Pacific Marine Science Organization, c/o Institute of Ocean Sciences, Sidney, British Columbia, Canada.
[2]Fisheries and Oceans Canada, Institute of Ocean Sciences, Sidney, British Columbia, Canada.

0148-0227/07/2006JC003671

semidiurnal tides, coincident with a maximum lunar declination. Tidal theory also predicts different variations with latitude for semidiurnal and diurnal constituents, with the former reaching maximum height on the equator and decreasing toward the poles, while the latter reach peak potential at 45° north and south of the equator [*Doodson and Warburg*, 1941].

[4] The LNC affects surface ocean temperatures via diapycnal mixing due to enhanced/diminished tidal currents according to the phase of the cycle [*Loder and Garrett*, 1978]. In most oceans the semidiurnal tides dominate the diurnal height by a factor of about two and semidiurnal currents dominate diurnal currents by a factor of about 4 to 5. The work done by tidal currents, which is generally proportional to mixing energy, varies as the cube of the tidal current [*Simpson and Hunter*, 1974]. Therefore, tidal mixing will be dominated normally by the semidiurnal tide, but LNC modulations in tidal mixing can be due to either diurnal or semidiurnal, depending on their relative strength. A thorough description of relative strengths of diurnal and semidiurnal mixing is discussed in Appendix A. We note here that each of the diurnal and semidiurnal tidal bands should contribute about the same modulation in mixing for tidal regimes in which the relative amplitudes of the two tidal bands follow the astronomical potential ratios. In regions with mixed but mainly diurnal regimes, the diurnal LNC will dominate; maximum diurnal tidal mixing occurred in 1950, 1968, 1987, 2006 and other years separated by 18.6 years. Ocean regions dominated by semidiurnal LNC attained peak mixing in 1959, 1978, 1997, etc. *Loder and Garrett* [1978] showed that on the Pacific coast of Canada one expects diurnal tidal mixing to determine the LNC signal, whereas in Atlantic Canada the semidiurnal tidal mixing should dominate. These differences will be roughly true for most of the North Pacific Ocean and North Atlantic as well.

[5] The precise astronomical periodicity of the LNC should allow its detection in century- or millenium-scale climate records because the LNC will emerge from other less-regular climate phenomena such as ENSO or the Pacific Decadal Oscillation [*Mantua et al.*, 1997]. The magnitudes of individual Fourier components of broadband noise decrease as the square root of the length of the record, whereas astronomical signals such as LNC with precise periods maintain constant Fourier amplitude, and eventually emerge above background noise in a sufficiently long record.

[6] Previous studies of oceanic and atmospheric time series have detected the LNC at various locations throughout the Pacific and elsewhere. In the northeast Pacific, it was first reported in approximately 35 years (1935–1970) of annually averaged shore station SSTs [*Loder and Garrett*, 1978], and later in a 172-year record of mean monthly surface air temperatures at Sitka, Alaska [*Royer*, 1993]. Evidence of the LNC signal in the tropics (~140 years of the Southern Oscillation Index and the Cold Tongue Index) is weak but the statistical power of these lengthy times series was sufficient to detect small effects [*Cerveny and Schaffer*, 2001]. A series of papers by Currie and coauthors, listed by *Currie* [1996], describes the LNC in many time series of geophysical data throughout the world. The low frequency oscillations of many physical parameters in the northwestern Pacific Ocean [*Ono et al.*, 2001; *Watanabe et al.*, 2003] are now considered to have their origins in the LNC [*Osafune and Yasuda*, 2006].

[7] This contribution to the study of LNC signals in the sea and the atmosphere re-examines the *Loder and Garrett* [1978] ideas for the northeastern Pacific with the benefit of thirty additional years of data, and with the benefit of being able to bring several instrumental and proxy temperature data sets to bear on the question. We expanded the *Loder and Garrett* [1978] domain from the shoreline out to the continental shelf bottom where tidal mixing is expected to take place, and into adjacent oceanic regions as well as onto land where the effects might also be felt. Representative indices of surface ocean and atmosphere temperatures were developed from monthly rather than annual means in consideration of the dominance of the seasonal cycle in subarctic regions. Subsurface current meters were examined to understand the relative contributions of diurnal and semidiurnal tides in vertical mixing on the British Columbia coast. Each of these instrumental temperature records was examined to assess their correspondence with the phase of the LNC. Proxy air temperature indices, previously developed from tree ring data, are also examined. All are discussed in relation to the contributions of local and remote tidal mixing to the regional LNC signal.

2. Data Sources and Analyses

2.1. Air Temperature

[8] The longest air temperature record in the northeastern Pacific is from Sitka, Alaska (57°N 135°W), where it appears that the Russian explorer Fedor Lütke left a thermometer during his stay there in the winter of 1827/28. A more complete description of this time series is given by *Royer* [1993]. Rather than rely on a single lengthy time series to represent interannual air temperature variation in the northeast Pacific, we obtained archival records of air temperature at all western Canadian meteorological stations and extracted those of the coastal province of British Columbia where the earliest systematic records began in 1872. These records include the observed daily minimum and daily maximum air temperatures and a computed daily average. For each station with at least a 19-year span of observations (a single LNC), mean monthly air temperatures were calculated as the average of daily minimum temperatures during each month. Daily minimum air temperatures were favoured over daily mean values as the former are observed values while the latter is a statistical compromise of the diurnal forcing. A cursory exploration of the effects of choosing daily minimums over daily means or maximums indicated a negligible effect on the results. Furthermore, daily minimum temperatures are more likely to be influenced by large-scale weather patterns; whereas average temperatures have additional influence from local solar heating. In what follows, references to monthly average air temperatures computed from this data set should bear in mind that they are computed from the daily minima, unless indicated otherwise.

[9] The data were stratified by calendar month to generate 12 subsets, each containing data for all stations. The history of record keeping at each station varies; starting years vary, some are no longer operating, some stopped observations

Table 1. Meteorological Stations With Lengthy Air Temperature Time Series Operating in 2000 in British Columbia

Station	Station No(s).	Latitude	Longitude	Elevation, m	Start Year
Gonzales (Victoria)	1018610	48° 25′	123° 19′	70	1899
Saanichton	1016940	48° 37′	123° 25′	61	1914
Shawnigan Lake	1017230	48° 39′	123° 38′	139	1911
Quatsino	1036570	50° 32′	127° 37′	2	1895
Bella Coola	1060840/41	52° 23′	126° 38′	35	1895
Hedley	1123360	49° 21′	120° 05′	540	1904
Vernon	1128550	50° 14′	119° 15′	379	1893
Westwold	1168880	50° 29′	119° 45′	617	1921
Fort St. James	1092970/72	54° 27′	124° 15′	695	1895
Golden	1173210	51° 18′	116° 58′	787	1902
Creston	1142160	49° 06′	116° 31′	636	1912
Kaslo	1143900	49° 55′	116° 54′	542	1894
Barkerville	1090660	53° 04′	121° 31′	1274	1888
Fauquier	1142820	49° 52′	118° 05′	445	1913
Fernie	1152850	49° 30′	115° 03′	1007	1913
Agassiz	1100120	49° 15′	121° 46′	46	1889
Lake Louise	3053760	51° 26′	116° 13′	1524	1915
Banff	3050519/20	51° 11′	115° 34′	1384	1888
Vavenby	1169520	51° 35′	119° 47′	447	1913

for variable periods. By month, correlations of monthly mean air temperature between any two stations were computed using all available years of data for the two stations (pairwise deletion), subject to an arbitrary criterion that station pairs have at least 10 years of overlapping observations. The resulting subset of 337 eligible stations produced a total of 3003 pairwise correlations for each month. Correlations between all station pairs were compared with the horizontal distances between stations (computed from Great Circle distances) to understand the correlation decay scale. Thereafter, 19 sites with the lengthiest and most complete time series (Table 1) were chosen for further analysis. The age and completeness of records from two additional stations (Banff 1888–2000 and Lake Louise 1915–2000) inspired their inclusion although they lie approximately 80 km and 10 km, respectively, beyond the British Columbia border. Nevertheless, they are highly correlated with British Columbia air temperature patterns. Principal component (PC) analyses were conducted with these 19 time series for each of the 12 calendar months independently to extract the dominant interannual history of air temperature variation shared among stations. Stratifying the analyses by month permits an examination of seasonal changes in the correlation structure.

[10] As the greatest correlation of air temperature with the LNC occurs during winter, we restricted most analyses to observations made in January, a month when solar declination events produced stronger tides at high latitudes [*da Silva and Avissar*, 2005]. The variable durations of these time series and the (infrequent) missing values within each series reduced the number of years with directly computable annual principal component scores from 113 to 63. Most of the missing values are from the 19th century when only 7 of the 19 selected sites (Gonzales, Quatsino, Bella Coola, Barkerville, Fort St. James, Agassiz, and Banff) were operating. Scores on PC 1 for the missing Januarys were estimated by multiple linear regression as 3.32 + BANFF * 0.10 + BARKERVILLE * 0.12) by exploiting the very high coefficient of determination (R^2 = 91%) between PC 1 and two of the longest series.

2.2. Sea Surface Temperature

[11] SST measurements have been recorded daily by lighthouse keepers stationed along British Columbia's coastline since the early 20th century (Figure 1). Each observation was taken at a time of local high water during daylight but we do not expect this tidal-solar-based timing of sampling to enhance or suppress the LNC signal in the

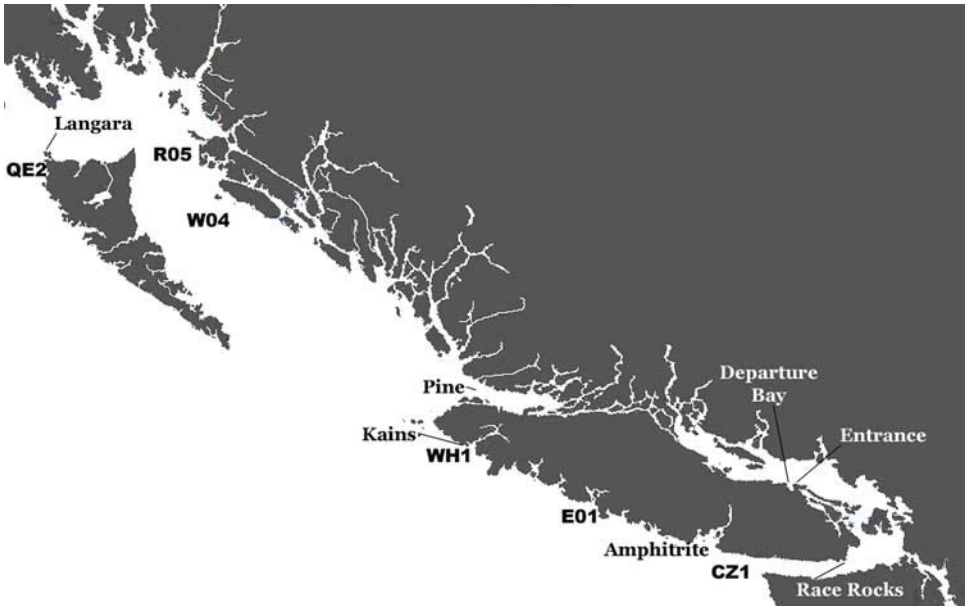

Figure 1. Locations of coastal lighthouses in British Columbia where daily temperature observations of temperature and salinity have been collected for over 70 years (since 1914 at Departure Bay). The locations of coastal near-bottom moorings are indicated by three digit codes.

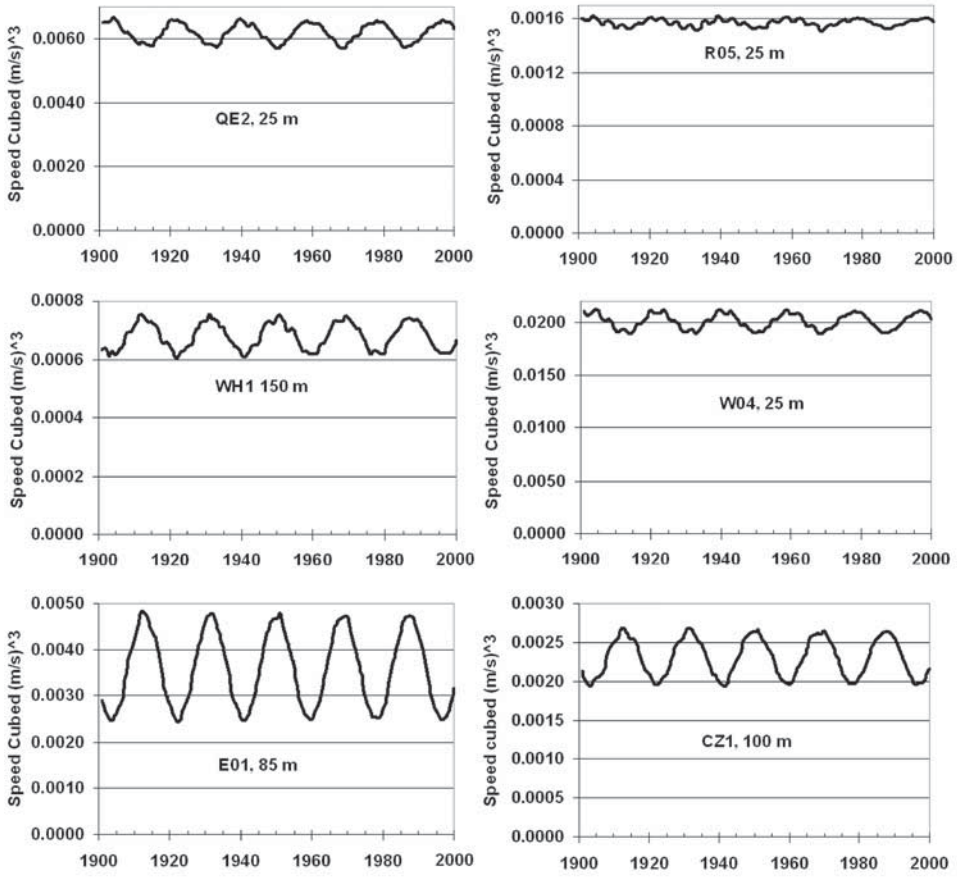

Figure 2. Time series of annual averages of the cube of the simulated hourly tidal current speed at six sites in British Columbia coastal waters.

records, although it may affect analyses of fortnightly modulations. These sites are located throughout the latitudinal range of about 48.5°N to 55°N, either on rocky points exposed to the open Pacific, or on small islands in areas of strong tidal mixing, or in regions bordering semienclosed seas and straits. When combined with similar shore station data from the United States, these measurements provide a rich source of pan-coastal time series to test hypotheses about physical mechanisms affecting coastal SSTs [*Tully et al.*, 1960; *Roden*, 1961; *Tabata*, 1985, 1989; *Roden*, 1989; *Lluch-Cota et al.*, 2001]. Average monthly SSTs were calculated for stations in Canada with the lengthiest and most complete records (Kains Island, Pine Island, Amphitrite Point, Race Rocks, Entrance Island, Departure Bay, and Langara Island). Unrotated principal component analysis of the monthly time series was conducted on pairwise correlation matrices. Focusing on the January results, rare missing scores on PC 1 were estimated from Pine Island SSTs as $-9.95 + \text{PINE} * 1.34$ ($R^2 = 88\%$). Pine Island has the highest loading on PC 1 in January.

[12] To compare the shore station results with SST variation offshore, the phase of the LNC was compared with gridded NOAA Extended Reconstructed SST data (http://www.cdc.noaa.gov/cdc/data.noaa.ersst.html). These data consist of time series of monthly SSTs from 1854–2002 (when obtained in late 2005) at each $2° \times 2°$ latitude/longitude grid point. While data quality may be poorer for the early portion of this time series due to a lack of observations, they should be adequate during these years to resolve an LNC signal due to its relatively long period. Anomalies at each grid point were calculated as deviations of a monthly mean from the overall mean for that month across the entire series. Grid points from the coast to 160°W and from the equator to 60°N were selected as the regional geographic scale of interest. Correlation coefficients of the LNC with each SST anomaly time series on the 2° grid in each month were examined closely to understand any seasonal effects on the correlations.

2.3. Ocean Currents

[13] Current meters were moored at many locations along the continental margin of British Columbia beginning in 1975, and many of these locations have more than one year of hourly or half-hourly observations. These provide sufficient information to compute theoretical LNC modulation of tidal current speeds, and to estimate modulations of mixing that are expected to vary as the cube of the tidal current speed. We selected representative stations with 12 or more months of observations and computed tidal constituents at each according to *Foreman* [1977]. Using these constituent sets, we computed 100 years of hourly records of the cube of the tidal current speed at each selected mooring, then calculated annual averages of the absolute value of the cubed current (Figure 2). Annual values of the

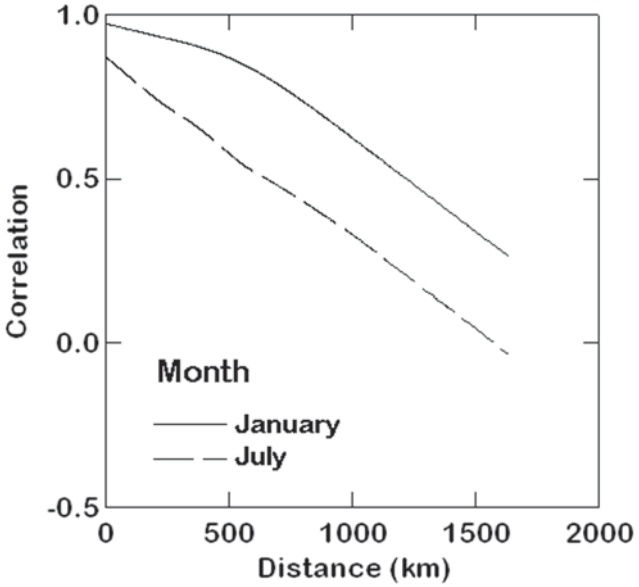

Figure 3. Loess trend lines showing how correlations in mean monthly air temperature among climate sites in British Columbia decline with increasing distance among sites in January (solid) and July (dashed). Sites used to prepare this figure had temperature histories of at least 19 years duration with at least 10 overlapping years between station pairs.

K1 tidal constituent were computed according to *Foreman* [1977] and used as an index of the influence of diurnal tides in each year.

[14] Cubed current speeds along the west coast of Vancouver Island (stations CZ1, E01 and WH1) are subjected to relatively large nodal modulation, in phase with the LNC, with the oscillatory component ranging from 65% of the average speed cubed at E01 to 32% at CZ1 and 22% at WH1. This portion of the BC continental margin is swept by tidally generated, diurnal period, continental shelf waves whose currents exceed those due to semidiurnal tides [*Crawford and Thomson*, 1984; *Crawford*, 1984]. Elsewhere the modulation is in phase with the semidiurnal tides, although without the higher frequency components found in Figure A1, and of smaller relative amplitude: 5% at R05, 11% at W01 and 13% at QE2. A similar calculation with the long period tidal components included revealed similar phases at every mooring, but the relative amplitudes of oscillating to average speed cubed was somewhat smaller. Tidal constants of monthly and fortnightly constituents are generally unreliable with only a year or so of data, and we have relied on predictions that do not include these constituents.

3. Results

3.1. Surface Air Temperature

[15] Mean monthly air temperatures at British Columbia stations tend to be more correlated in January than in July (Figure 3) and the magnitude of the correlation decreases with increasing distance between stations. For stations located less than approximately 600 km apart, the spatial de-correlation scale was greater in January than in July because of the greater spatial scale of winter weather systems (Pacific lows or Arctic highs). Beyond 600 km, the correlations decline at approximately the same rate with increasing distance. Following from these results, subsequent analysis is focussed on January data when the covariation among stations has its greatest spatial scale, and when the LNC signal in temperature data is most apparent.

[16] A principal component analysis of average January air temperatures at 19 sites distributed throughout central and southern BC indicated that most of the interannual variation was shared commonly by all stations. The first principal component [hereafter identified as *PC* 1 (*air*)] accounted for 89% of the variance in the pairwise correlation matrix. Loadings on *PC* 1 (*air*) ranged from a low of 0.87 at Creston to a high of 0.98 at Vernon, Gonzales (Victoria), and Westwold. The frequency distribution of *PC* 1 (*air*) is bimodal due to the infrequent, but characteristically different, years of significantly greater Arctic influence. These strong outbreaks of the Arctic air mass in winter depress regional temperatures below the typical range in January. They also increase the magnitude of correlations among stations and consequently, affect the magnitude of the eigenvalue associated with the first eigenvector (Figure 4).

[17] Much of the interannual variation in January air temperatures in the northeast Pacific since 1950 can be attributed to interannual variation in hemispheric-scale climate patterns in that month (Table 2). At Sitka, Alaska, for example, the correlation of mean January air temperature with the PNA teleconnection index [*Barnston and Livezey*, 1987] is 0.85, declining to a low of 0.04 in June. A comparison of the PNA index with average monthly air temperatures at British Columbia stations (Table 1) in all

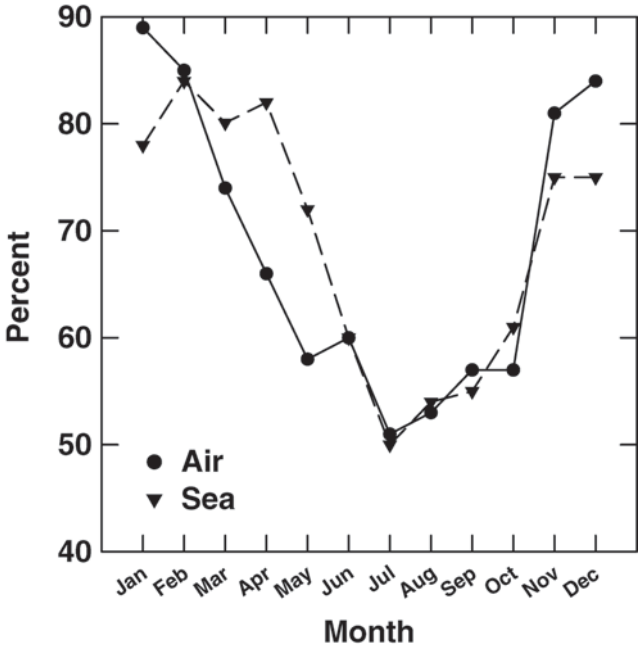

Figure 4. Percentage of the variance of monthly mean sea surface temperatures (dashed) and monthly mean (of daily minima) air temperature (solid) among years attributed to the dominant principal component. Temperatures are more correlated among stations in winter than summer for both air and sea temperatures.

Table 2. Correlations at Lag Zero and Their Significance Levels of *PC* 1 (*air*) Scores and *PC* 1 (*sea*) Scores With Large-Scale Climate Indices and the Lunar Nodal Cycle From 1937 to 2000 (2006 for the PNA) for the Month of January[a]

Index (Jan Values)	*PC 1 (air)*	*PC 1 (sea)*
Pacific/North American Pattern	+0.70 ($P < 10^{-6}$)	+0.70 ($P < 10^{-6}$)
North Pacific Index	−0.60 ($P < 10^{-6}$)	−0.65 ($P < 10^{-6}$)
Pacific Decadal Oscillation	+0.50 ($P < 10^{-4}$)	+0.72 ($P < 10^{-6}$)
Southern Oscillation Index	−0.21 ($P < 0.18$)	−0.32 ($P < 0.03$)
Multivariate ENSO Index – Dec/Jan	+0.21 ($P < 0.14$)	+0.43 ($P < 0.002$)
K_1 tidal constituent	−0.15 ($P < 0.29$)	−0.31 ($P < 0.012$)

[a]Pacific/North American Pattern [*Barnston and Livezey*, 1987] (http://www.cpc.noaa.gov/products/precip/CWlink/pna/norm.pna.monthly.b5001.current.ascii), North Pacific Index [*Trenberth and Hurrell*, 1994] (http://www.cgd.ucar.edu/cas/jhurrell/indices.html), Pacific Decadal Oscillation [*Mantua et al.*, 1997], Southern Oscillation Index (http://www.bom.gov.au/); Multivariate ENSO Index [*Wolter and Timlin*, 1998] (http://www.cdc.noaa.gov/people/klaus.wolter/mei/mei.html), K_1 tidal constituent [*Foreman*, 1977].

months indicates that the magnitude of this correlation has a strong annual cycle, peaking in December (average r = 0.65 among BC stations) and reaching a minimum (uncorrelated) during summer. The correlations were consistently greater at the northernmost stations (e.g. Ft. St. James, r = 0.77) and weakest at the easternmost stations (e.g. Lake Louise r = 0.48). Two stations (Atlin: r = 0.79 and Mayo: r = 0.85) that are located northeast of Sitka and therefore were not used in determining *PC* 1 (*air*), have the same high correlation with the PNA in January as Sitka.

3.2. Coastal Sea Surface Temperature

[18] Mean monthly SST correlations among coastal British Columbia shore stations are highest during the late winter months, peaking in February/March, and lowest in summer (Figure 4). Unlike air temperatures that show a pronounced peak correlation in January, the period of higher correlation among stations persists into early spring. During winter, these SSTs are also highly correlated with SSTs throughout much of the Gulf of Alaska [*McGowan et al.*, 1998; *McKinnell et al.*, 1999]. A principal component analysis of mean January SSTs at shore stations indicated that, as with air temperatures, all stations share a common interannual pattern. *PC* 1 (*sea*) accounted for 78% of the variance of the pairwise correlation matrix in January. Although this was 11% less than for air temperatures in the same month, half of the difference was due to the inclusion of two stations located within Georgia Strait which is connected with the Gulf of Alaska only through two narrow passages at its northern and southern extremes. Correlations between *PC* 1 (*sea*) and individual time series (loadings) varied in strength from a low of 0.85 (Entrance Island, located in Georgia Strait) to 0.93 (Pine Island, located in Queen Charlotte Strait). Pine Island is one of two stations (Race Rocks is the second) located in straits with a substantial influence of tidal mixing on SSTs; this warrants further attention but will not be addressed in this work.

[19] The correlation between *PC* 1 (*air*) and *PC* 1 (*sea*) in January from 1937 to 2000 is 0.77 (Figure 5) and it varies seasonally (e.g. March: 0.37, May: 0.24, July: 0.42, September: 0.17, November: −0.04). When *PC* 1 (*air*) and *PC* 1 (*sea*) in January were compared with other common large-scale climate indices for the same period (Table 2), all had lesser correlations than the *PC* 1 (*air*) – *PC* 1 (*sea*) correlation. The highest correlation of air or sea temperature series with large scale climate indices was between *PC* 1 (*sea*) and the PNA index (r = 0.73), indicating a good correspondence between the state of North Pacific teleconnection and local surface temperatures in January. Average wind vectors at 700 hPa during the most extreme cold and warm years (1950, 1981) provide an indication of the nature of the association (Figure 6). January of 1950 was the coldest of the century along the west coast. It was associated with strong easterlies at the

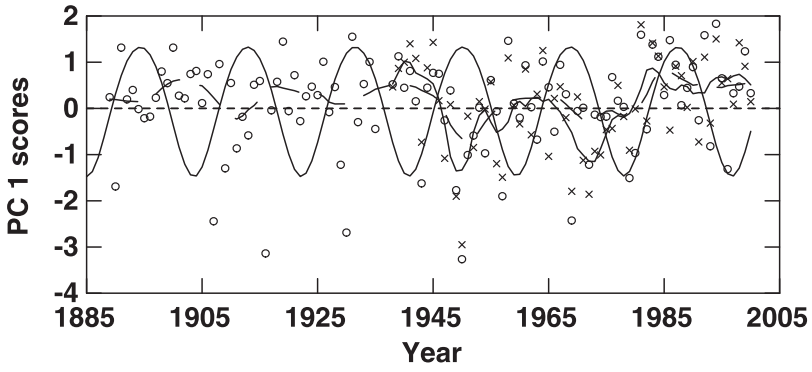

Figure 5. Principal component scores for average air temperature (open circles, solid loess trend line), and average monthly sea surface temperatures (crosses, dashed loess trend line) in January in BC. *PC* 1 (*air*) accounts for 89% of the variation in the among-site correlation matrix and *PC* 1 (*sea*) accounts for 78% of the variation in the among-site correlation matrix. The correlation between the two January series from 1937 to 2000 is r = 0.77. The phase and period of the diurnal lunar nodal cycle is indicated by a solid line.

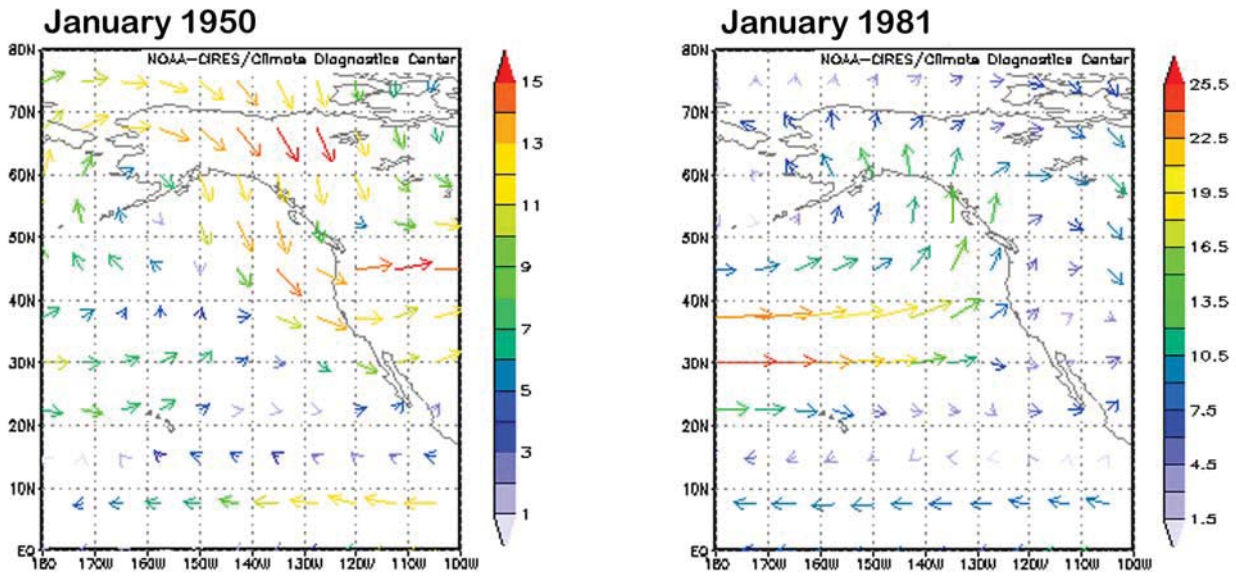

Figure 6. Speed/direction vectors for average January 700 h-Pa winds. The years selected are the lowest (1950) and highest (1981) values of the January PNA index from 1950–2006. Color legends indicate average speeds (m s^{-1}). These years are also the coldest and warmest average January sea and air surface temperatures in British Columbia. Plotted panels are courtesy of the NOAA-CIRES Climate Diagnostics Center in Boulder, Colorado, from their website at http://www.cdc.noaa.gov/.

equator from enhanced Walker circulation, a shutdown of the mid-latitude westerlies and enhanced northerly winds over western North America. January of 1981 had strong mid-latitude westerlies and strong southerly winds over western North America.

[20] Lengthy air and sea temperature time series are of interest to studies of global climate change and global warming. While the hemispheric temperatures have been rising, there is no statistically significant long-term linear trend in either *PC* 1 (*sea*) ($P < 0.14$, $n = 64$) or *PC* 1 (*air*) ($P < 0.52$, $n = 111$) in this region in the month of January. What is noteworthy, however, is a lack of cold Januarys since the climate shift in 1976/77.

3.3. Lunar Nodal Cycle and Instrumental Temperatures on the West Coast

[21] There is a significant correlation between *PC* 1 (*sea*) and the LNC ($r = -0.31$, $P < 0.02$) at zero lag, and the correlation increases to a slightly larger peak at $r = -0.39$ at a two year lag (not shown), LNC leading ($P < 0.002$). The correlation of the LNC with *PC* 1 (*air*) has the same sign as *PC* 1 (*sea*) ($r = -0.16$) and the same correlation peak at a two year lag, but is not statistically significant. January air temperatures at all 19 of the individual stations in British Columbia are negatively correlated with the LNC but only at Agassiz, Bella Coola, Gonzales, and Quatsino are they statistically significant ($P < 0.05$). Of these, only Agassiz is not located at the shoreline.

[22] In contrast to what is observed in British Columbia, the cross-correlation peak ($r = -0.41$, $P < 0.0002$) between the LNC and mean January SSTs at Scripps Pier (La Jolla, CA) occurs at zero lag, although the correlations are also significant when lagged for a few years. The most extreme positive SST anomalies in winter at Scripps Pier always occurred during an LNC minimum and the lowest SST anomalies frequently, but not always, occurred within a year or two of an LNC maximum (Figure 7). Gridded 2° latitude × 2° longitude SSTs off the U.S. west coast in winter (January and February) are correlated with the LNC over a broad spatial extent for a period of 150 years (Figure 8). The strength of the correlation, which again is greatest in January, varies in magnitude according to the particular grid point chosen, reaching its largest magnitude ($r = -0.39$, $P < 10^{-6}$) at 40°N 130°W. The correspondence between the LNC and the temporal trajectory of the 5-year moving average of these SSTs is clearly evident as higher (lower) average temperatures when diurnal tides are weaker (stronger) within cycles (Figure 8). Departures from this cyclical pattern (e.g. late 1870s and the early 1920s) are rather rare. An intriguing feature of the spatial pattern of these correla-

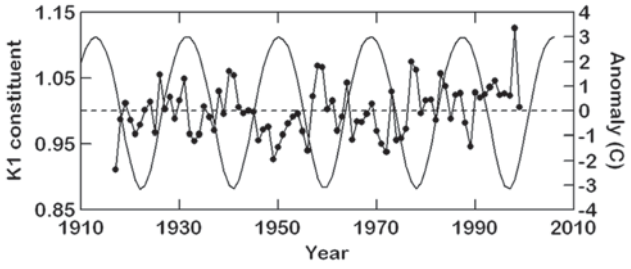

Figure 7. Mean January sea surface temperatures anomalies (departures from the 1917–1999 January mean) at Scripps Pier (solid circles) superimposed on the diurnal lunar nodal cycle.

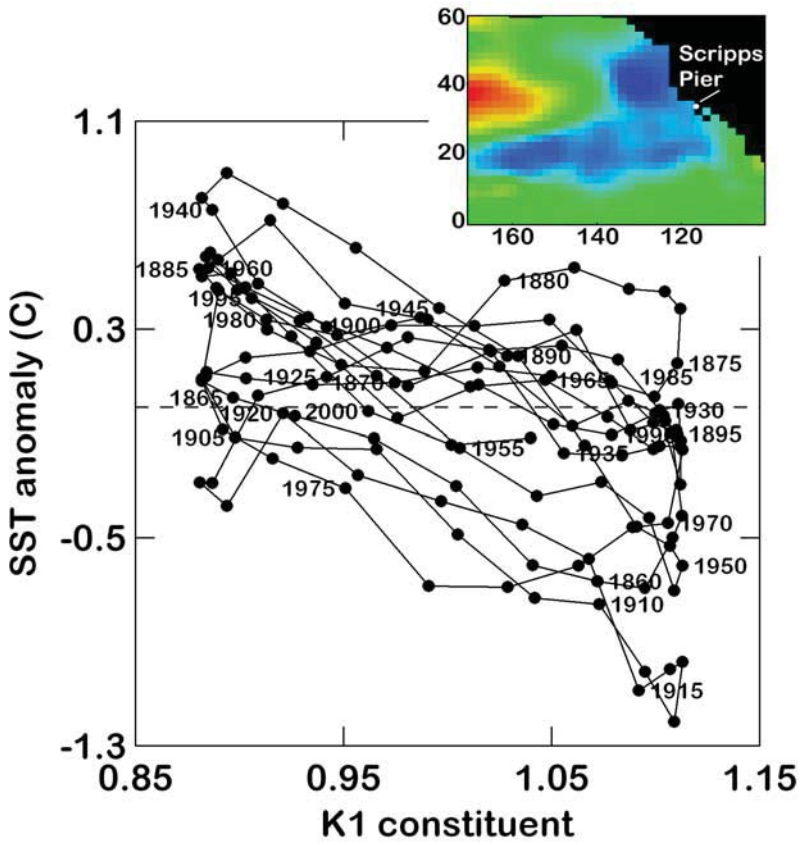

Figure 8. Bivariate plot of a 5 year moving average of January SST anomalies at 40°N 130°W versus the 18.6 year lunar nodal cycle. Point labels for every fifth year in the time series indicate the year at the centre of the 5 year moving average. The solid line connects adjacent years from the start of the time series in 1854 to its end in 2002. The line is intended to show a trajectory of how SSTs tend generally to cycle from low values during peak diurnal tides to high values during small diurnal tides. The inset shows the spatial pattern of the LNC ⟨ ⟩ SST correlation in January off the west coast of North America and its relation to Scripps Pier.

tions (Figure 8, inset) is its resemblance to the spatial scale of the California Current System, at least from the Oregon coast to the subtropics. The maximum is located near at least two potentially relevant features. The climatological mean of the North Pacific high pressure system is located at 35°N 130°W [*Schwing et al.*, 2002], 5° of latitude south of the maximum correlation. Nevertheless, there is no significant correlation of January SST here with the Northern Oscillation Index. The second feature is an abrupt and extreme change in deep topography, the Mendocino Escarpment, at the latitude of highest correlation, but we have no evidence of how it might be involved.

[23] Using instrumental air temperature records of slightly longer duration than are available in British Columbia, *Roden* [1989] identified many periods of persistently warm or cold air temperature anomalies along the west coast of North America from San Diego, CA to Sitka, AK. Some stanzas were linked to known causes but some (warm: 1864–1870, 1940–1945, 1977–1984 and cold: 1857–1863, 1946–1956) could not be explained by the phenomena he considered, and the LNC was not among them. Yet when these stanzas are superimposed on the LNC, it becomes readily apparent that all of Roden's unexplained anomalies correspond with what might be expected from the state of the LNC (Figure 9). The probability of these warm and cold stanzas aligning randomly with this degree of correspondence (or better) to the phase of the LNC is <0.006. The method for determining this probability is described in the next section on proxy temperatures and the LNC.

[24] At the British Columbia (and one Alaska) stations examined in this study, the relationship between monthly values of the PNA index and average monthly air and sea temperatures is essentially linear and dominant in winter, abating to uncorrelated in summer. As the expression of both the PNA and the LNC are strongest in winter, it begs the question of whether the correlations of temperature with the LNC arise as a consequence of some form of physical connection between the LNC and the PNA, or whether they are independent of each other. If there was such an influence, the dominant role of the PNA pattern in determining northeast Pacific surface temperatures in winter provides an alternative mechanism for the appearance of the LNC signal in the northeast Pacific. At zero lag, the correlation between the LNC and the January PNA index is not significant ($r = -0.19$) over the period 1950–2006. However, the PNA begins to have a statistically significant correlation ($r = -0.34$, $P < 0.01$) with LNC at a two year lag (Figure 10). This is the

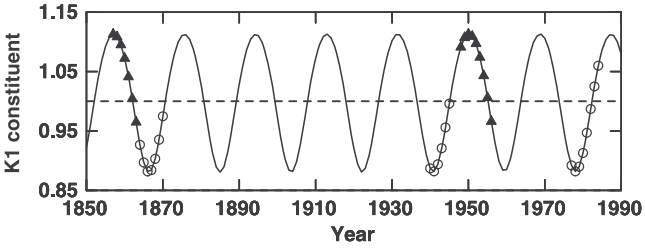

Figure 9. Stanzas of persistently warm (open circles) or persistently cold (solid triangles) annual air temperatures along the west coast of North America between 1850–1990 with no known cause [*Roden*, 1989]; superimposed on the phase and amplitude of the K_1 diurnal tidal constituent (the continuous line). These unexplained warm stanzas occurred with $K_1 < 1.0$ and all cold stanzas occurred when the constituent was high with only four individual years not matching this pattern. The likelihood of an agreement of this degree of correspondence or better between the occurrence of these five stanzas and the phase of lunar nodal cycle arising by chance is $P < 0.006$.

same lag that appears in the northern northeast Pacific temperature time series.

[25] The apparent dominance of the PNA in these temperature series implies a need to account for the PNA when interpreting any simple correlation between the LNC and temperature. If the influence of the January PNA index is removed from *PC* 1 (*air*) by stepwise regression, none of the residual variance is explained by the LNC ($P < 0.36$). A similar result is obtained when *PC* 1 (*sea*) is used ($P < 0.81$) meaning that the LNC signal in the sea is not independent of the PNA. Even at Sitka, where the LNC was first detected in the air temperature frequency domain [*Royer*, 1993], the LNC fails to explain any residual variance in January air temperatures ($P < 0.62$), after removing the influence of the PNA. In summary, these results suggest that the LNC signal in these temperature series is not independent of the PNA but a component of the PNA.

3.4. Lunar Nodal Cycle and Temperature Proxies (Tree Rings)

[26] Co-occurrences of warm/cool temperature anomalies with the corresponding phase of the LNC are unlikely to be spurious if they persist for centuries. *Ware and Thomson* [2000] studied nearly 400 years of mean annual temperature data (1604–1984) reconstructed from tree rings [*Fritts*, 1991] and identified six extreme warm and six extreme cool stanzas at two sites (Vancouver, BC and Sacramento, CA). While the duration of these stanzas varied from 4–11 years, each had the property of being either persistently warm or cold for a few years such that the integrated anomaly over the stanza was larger than other such groups of years in the time series. We superimposed the timing of these warm/cool stanzas on the LNC to reveal that all six of the Vancouver warm periods (Figure 11) and five of six of the Sacramento warm periods (not shown) occurred when the LNC was in its minimum phase ($K_1 < 1.0$). The likelihood of this occurring by chance can be likened to obtaining six ''heads'' in six tosses of a coin if one considers whether a stanza occurs during two potential states of the LNC (i.e. $K_1 < 1.0$ or $K_1 > 1.0$). As a more rigorous test of hypothesis involving both the cool and warm stanzas, we used Monte Carlo methods to address the question: what is the probability of obtaining an arrangement of six warm and six cool stanzas, maintaining their observed durations, by chance with this degree of correspondence (or better) with the LNC. At Vancouver, the durations of cold stanzas were 11, 8, 5, 6, 5, and 7 years and the durations of warm stanzas were 9, 7, 5, 7, 4, and 4 years. According to the LNC, cooler temperatures are expected during years with $K_1 > 1.0$ and warm temperatures are expected with $K_1 > 0$. Evidence against the LNC as the cause of temperature anomalies grows as the probability of such matches occurs by chance alone. We tested the hypothesis that the observed correspondence occurred as a random result by writing a Monte Carlo program that, on each iteration, randomly selected a starting year for each of the 12 observed stanzas such that all were accommodated, without overlap, within the period of the temperature reconstruction (1604–1984). The number of mismatches of individual years with the state of LNC in that year was computed on each iteration. A mismatch was defined as a year when a cool (warm) stanza occurred in a year with $K_1 < 1.0 (K_1 > 1.0)$. The total number of mismatched years observed in the Vancouver data is 21. The procedure was repeated 100,000 times, each time recording the total number of mismatches that arose by chance. The result of the test was that only 1.5% of the trials produced the observed number of mismatches or fewer by chance. In common statistical practice, 5% is sufficient to reject the hypothesis of a correspondence occurring by a chance occurrence. When computed with the characteristics of the Sacramento temperature stanzas, the outcome favoured

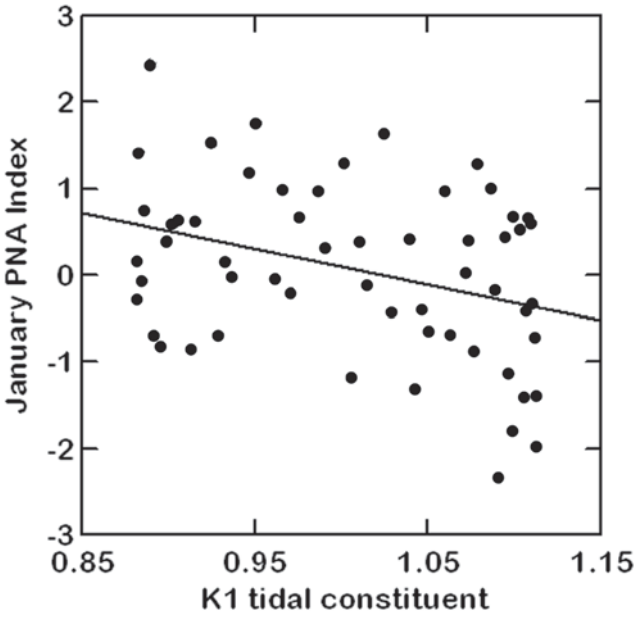

Figure 10. Magnitude of the PNA index in January from 1950–2006 (positive is warm over western North America), versus the magnitude of the diurnal tidal constituent, K_1, two years earlier. The solid line shows the linear trend in these data. The correlation between the two is ($r = -0.35$, $P < 0.01$).

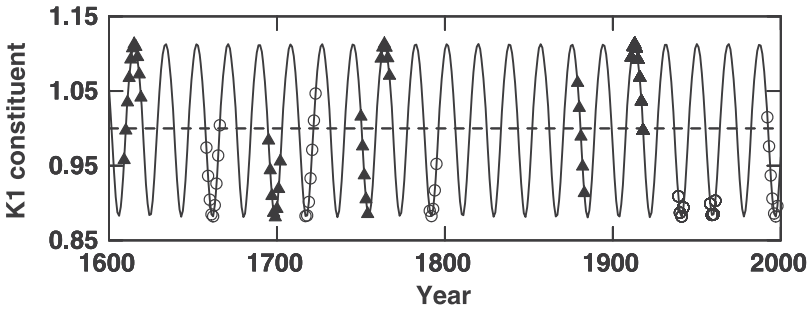

Figure 11. The phase and amplitude of the K_1 constituent from 1600 to 2000 is indicated by the continuous cycle based on calculations from *Foreman* [1977]. Mixing by diurnal tides is lower when the constituent has values <1.0 and greater otherwise. Superimposed on this cycle are stanzas (short sequences of years) of persistently warm annual temperature anomalies (open circles) or cold annual temperature anomalies (solid triangles) that occurred between 1602 and 1984. Note that no warm stanzas were centred over years when diurnal tides were most energetic, while cold phases occurred during either phase of the lunar nodal cycle.

rejection of the hypothesis but the result was not statistically significant (P = 7.9%). The difference between Vancouver and Sacramento was primarily because the warm stanza of the late 1700s occurred a few years later in the Sacramento data than in the Vancouver data. The offset produced an increased number of mismatches at that site.

4. Summary of Results

[27] 1. Average air and sea surface temperatures in British Columbia and southeast Alaska in January are determined largely by winds associated with the state of the Pacific/North American atmospheric pattern in January.

[28] 2. There is a significant correlation of the LNC with January SSTs in coastal British Columbia [*PC* 1 (*sea*)] and with mean January air temperatures in Sitka, Alaska, but not with the dominant component of January air temperature variation in British Columbia [*PC* 1 (*air*)].

[29] 3. Cross-correlations of these temperature series with the LNC are maximum at a two year lag, LNC leading, but they are not statistically significant after accounting for the state of the PNA in January.

[30] 4. There is a significant correlation of the PNA with the LNC at a two year lag, LNC leading, suggesting that the LNC signal is a component of the PNA rather than independent of it.

[31] 5. There is a significant correlation of the LNC with January SSTs at Scripps Pier and with January SSTs in the California Current system generally.

[32] 6. January SSTs at Scripps Pier can be described as a combined function of the multivariate ENSO index (47%), the LNC (17%), and the PNA (2%). The peak correlation with the LNC occurs at zero lag.

[33] 7. SST variation at the location of peak correlation with the LNC in the California Current is a function of the LNC (31%), multivariate ENSO index (8%) and the PNA (4%). The peak correlation with the LNC here is at 1 year lag.

[34] 8. Persistent extreme anomalies in 400 years of proxy annual temperatures obtained from tree rings indicate that the correspondence between the phase of the LNC with all of the warm stanzas and some of the cold stanzas at Vancouver was unlikely to have occurred by chance ($P < 0.016$) whereas the agreement at Sacramento was not so good ($P < 0.08$).

[35] 9. The PNA is uncorrelated with the LNC at zero lag but is (significantly) negatively correlated with the LNC at two to four year lags.

5. Discussion

[36] Evidence of the influence of the LNC on climate of the northeast Pacific was encountered first in annual average sea surface temperature at the west coast of Vancouver Island [*Loder and Garrett*, 1978] and later in the frequency domain of air temperature variation at Sitka, Alaska [*Royer*, 1993]. Although the physical mechanism for the cyclical component of these coastal surface temperatures was never demonstrated, it was inferred that the LNC arose from dissipation arising from local modulations of diapycnal mixing by the variable magnitude of diurnal tidal currents in the relatively shallow coastal ocean. The main difficulty with this hypothesis is that large diurnal tides are not common in the northeastern North Pacific, especially along the U.S. west coast [*Foreman et al.*, 2000; *Egbert and Erofeeva*, 2002]. *Foreman et al.* [2006] have developed numerical simulations to show that significant and dominant dissipation in the diurnal tides occurs along the Aleutian Islands. We might anticipate that the LNC will provide a connection of this dissipation to sea and air temperatures in British Columbia and the California Current through recirculation in the Alaska Gyre of the Gulf of Alaska, or through a link in the atmosphere to the Aleutian Low, but we have no direct evidence of these effects.

[37] The lack of specific mechanisms has fostered a general impression that the phenomenon is spurious and need not be considered as a factor responsible for climate variation in the North Pacific. While simple correlations of the LNC with coastal sea surface temperatures in British Columbia and with air temperatures in southeast Alaska in January are relatively weak, the correlations have persisted through nearly 30 years of additional observations since the phenomenon was first described. It seems clear that the winds associated with the PNA teleconnection are the

dominant source of winter temperature variation in the northern northeast Pacific. The results of the regression analysis indicate that the LNC correlation with surface temperature is not independent of the effects of the PNA on surface temperature, suggesting that the correlation arises as a component of the PNA. The co-occurrence of the two year lag in both the LNC ⟨ ⟩ PNA correlation and the LNC ⟨ ⟩ temperature correlations and the dominant role of the PNA in the northern northeast Pacific suggests an atmospheric link to the LNC in the northern northeast Pacific. The lack of a statistically significant correlation between the LNC and PNA in British Columbia [*PC* 1 (*air*)] might arise from a weakening influence of the PNA with decreasing latitude.

[38] The challenge now is to confirm how a low frequency modulation of tides might generate such a large spatial pattern. The key element of any hypothesis along these lines is that the mechanism must have a scale and geographic location to affect the global climate. Two qualifying sources of remotely generated temperature anomalies at this frequency are the Okhotsk Sea and the Indonesian archipelago where diurnal tides are large. The Okhotsk Sea has a significant role in the formation of North Pacific Intermediate Water. The fortnightly modulation of diurnal tides in the Okhotsk Sea is sufficient to influence the dynamics of polynyas over much of Kashevarov Bank in winter [*Rogachev et al.*, 2001], and annual spring air temperatures around the Okhotsk Sea have a strong LNC tidal signal (K. Rogachev, Pacific Oceanological Institute, personal communication). Furthermore, forty years of sampling in the Oyashio Current region, located downstream of the Okhotsk Sea, has identified a strong bidecadal oscillation signal of the correct phase and period for the LNC in waters found at depths normally associated with North Pacific Intermediate Water [*Ono et al.*, 2001; *Watanabe et al.*, 2003]. They found that average oxygen and phosphate concentrations had significant oscillatory components with periods estimated as 18.5 ± 1.0 y and 19.7 ± 1.4 y for oxygen and phosphate, respectively, at depths above $27.4\sigma_\theta$ (<1030 m). They also found similar signals in deeper waters of the northwestern Pacific and in the Japan/East Sea. The phase shift relative to the LNC appears to be the two year lag that appears in the northern northeast Pacific. *Yasuda et al.* [2006] and *Osafune and Yasuda* [2006] examined the LNC connection in these and other time series in much greater detail and presented rather convincing arguments for an LNC signal on a broad scale in the northwestern Pacific Ocean.

[39] Tidally induced variability in SSTs in the Indonesian archipelago appears as a fortnightly signal in rainfall in the western tropical Pacific [*Ffield and Gordon*, 1996], a region that is an important source of variability in the global climate system [*Qu et al.*, 2005]. The modulation of diurnal tides in parts of the western tropical Pacific, and their influence on heat fluxes and convection in that region provides a mechanism whereby the LNC could affect the global climate system, i.e. by being particularly influential in a critical region. Unlike the Okhotsk Sea, strong evidence of a bidecadal signal in the western tropical Pacific is lacking for the time-being although we note a phase match of the LNC and some of the largest El Niños (1940/41, 1957/58, 1997/98) of the 20th century. It is clear that one cannot attribute the cause of El Niños to the moon because some (e.g. 1972/73, 1982/83) are not in phase with the LNC but it might be instructive to explore their differences to resolve the nature of the lunar signal in the El Niño data that was first described by *Cerveny and Schaffer* [2001].

[40] The role of the PNA pattern in determining mean January air and sea temperatures diminishes with decreasing latitude along the North American coast. At the latitude of Scripps Pier, regression results suggest that the influence of the PNA pattern drops to only 4% of the variance in mean January SSTs while the influence of ENSO becomes dominant ($r = -0.69$, $P < 10^{-6}$). *Lluch-Cota et al.* [2001] noted the increasing influence of ENSO-scale variability in coastal SSTs with decreasing latitude along the North American coast. A second feature of variability in the January Scripps Pier SST data is the lack of a two-year lag in the LNC > SST cross-correlation. This suggests that the proximate mechanism for the appearance of the LNC in Scripps Pier SSTs may not be the same as that in British Columbia and Southeast Alaska. Furthermore, the regression results involving January SSTs at Scripps Pier indicated that at least some of the influence of the LNC was independent of the ENSO index in that month.

[41] One consequence of examining this issue using monthly data was to note that correlations of sea and air surface temperatures with the LNC are most apparent during winter months, especially January, perhaps due to stronger heat transfer between ocean and atmosphere in mid-and high-latitude winters and/or because the PNA and ENSOs are best developed at this time. We note that often only the largest temperature anomalies, either positive or negative, are in phase with the LNC. It is as though the phase of the LNC might establish a predisposition toward a corresponding temperature anomaly in winter, but whether or not it occurs depends upon the relative influence of all factors that affect surface temperatures.

[42] A fascinating aspect of our study was the identification of SST ⟨ ⟩ LNC correlations in winter off the U.S. west coast that are essentially the geographic scale and location of the California Current System. The surface waters of the California Current System in winter oscillate from warm to cool in phase with the LNC. This is could easily be the source of the LNC signal that can be detected at Scripps Pier. The question then becomes whether the California Current System in winter is the source of the temperature anomalies in the northeastern Pacific, or whether it is a consequence of forces applied elsewhere, as appears to be the case in the northwestern Pacific [*Yasuda et al.*, 2006]. The key features in this discussion are the apparent zero lag between the phase of the LNC and the SSTs in the California Current System and the current knowledge that ocean mixing by diurnal tides is thought to be rather weak along the narrow continental shelf of the U.S., south of Vancouver Island. *Foreman et al.* [2000] analyzed tidal dissipation in the Gulf of Alaska based on a finite-element, barotropic tidal model with 51,000 nodes, where the closest spacing of nodes occurred in shallow coastal regions. Both dissipation and mixing vary as the cube of the tidal current, and one can use dissipation as a general scaling factor for vertical mixing of heat and nutrients [*Crawford*, 1991]. Plate 5 of *Foreman et al.* [2000] displays a contour map for the northeast Pacific of both M_2 and K_1 dissipation north of 45°N and west to 160°W. Diurnal dissipation exceeds

semidiurnal dissipation only along the west coast of Vancouver Island, attributed to local diurnal-period, tidally driven shelf waves. A map of dissipation along the coast between 30°N and 45°N (M. G. G. Foreman, personal communication, 2001) shows very low dissipation for both semidiurnal and diurnal currents, to an extent that local tidal mixing in these waters is not likely a factor in temperature changes over periods of years.

[43] We and various authors have analysed lengthy time series of air and sea temperature observations in the Pacific Ocean in various ways at various spatial scales. Without exception, these studies showed that the bidecadal component of variability is present in the instrumental and proxy records. In their assessment of SST persistence throughout the entire Pacific Ocean, *Chao et al.* [2000] advanced this idea by noting that the bidecadal component appeared to be deterministic in nature and that it had a large spatial scale. Our contribution was to show that both the phase and period of the bidecadal component in the instrumental record was that of the 18.6-year LNC and that it also appears in proxy temperatures of up to 400 years in duration. *Yasuda et al.* [2006] have taken an important first step in translating correlation to plausible hypothesis linking the LNC to large-scale physical processes that are important to climate by showing how the LNC can affect the formation of North Pacific Intermediate Water and large-scale heat transfer in the western North Pacific. We also note that the response of North American coastal SSTs to many major El Niños of the 20th century are confounded with the SST response anticipated by the LNC. This unlikely coincidence will attract greater attention if a major El Niño occurs around 2015. The role of internal tides and diapycnal mixing in the ocean is far from certain [*Garrett*, 2003].

Appendix A: Tidal Modulation of Ocean Mixing

[44] Regions of the ocean with strong tidal currents are usually characterized by low surface temperatures, due to tidally driven turbulence that mixes cold, deep water to the surface. *Simpson and Hunter* [1974] examined this effect in the Irish Sea, noting that regions of relatively strong tidal currents were characterized by uniform temperatures from surface to bottom, and cooler surface waters in summer. They derived the factor H/U^3 to determine the presence of these vertically well mixed regions, where H is the water depth and U the peak tidal current speed. Low values of H/U^3 imply relatively strong mixing and weak or no stratification. This formula attributes spatial variability in mixing to the third power of the tidal current. The cubic relation arises from a tidal power transfer term, which is the product of quadratic friction at the ocean bottom (U^2) multiplied by the speed of the flow (U). Therefore tidal mixing will be highly sensitive to small changes in tidal current speeds, both in time and in space.

[45] In this paper we describe a search through climate records for effects that might be attributed to changing tidal current speeds caused by interannual variability of the lunar orbit. Both the point of closest approach of the moon to the Earth (perigee) and the point where the lunar orbit crosses the ecliptic (ascending lunar node) rotate slowly around the Earth with periods of about 8.85 and 18.61 years, respectively. The 18.6-year rotation of the lunar ascending node is associated with an oscillation of the lunar declination over the range ±5° relative to the 23.5° tilt of the equator relative to the ecliptic. Expressed in other words, the maximum monthly declination of the moon above the equator varies from about 18.5° to 28.5° and back over an 18.6-year cycle. The diurnal tides are set up by this tilt of the lunar orbit, and biggest diurnal tides are found during years of maximum lunar declination. As the lunar orbit tilts farther away from the equator, the semidiurnal tides diminish somewhat, and their lunar modulation is relatively small and out of phase with the diurnal modulation. The two largest diurnal tidal constituents, K_1 and O_1, reach peak values at the maximum lunar inclination of 28.5°, which last took place in late 1987 [*Schureman*, 1940] and in 2006. M_2, the largest semidiurnal tide, modulates by only 5° and last peaked in 1997.

[46] Modern computer tidal prediction algorithms compute the nodal modulation implicitly. For example, the *Foreman* [1977, 1978] algorithms assign constituent status to tidal signals that vary in frequency from the neighboring constituent by at least one cycle per year. A tidal constituent is a cosine wave whose period is defined by astronomical forcing, and whose phase and amplitude is determined by both the strength of astronomical forcing and the response of an oceanic basin. The main solar (S_2) and lunar (M_2) constituents are set up by astronomical forces as the moon orbits the Earth and the Earth orbits the Sun. These forces vary in time due to other factors, such as distance to Sun and moon, and declination of Sun and moon. Each of these effects is accounted for by another constituent, which is a cosine function at separate period and amplitude and phase. For example, the constituents that differ in frequency by one cycle per year are calculated by the Foreman algorithms if the observational record is at least one year in duration. If neighbouring tidal constituents differ in frequency by less than a cycle per year, constituent status is assigned to the larger, and the smaller constituent is considered to modulate the larger, at a period longer than one year.

[47] The height of the *n*th tidal constituent can be defined as a cosine function

$$h_n = f_n h_{on} \cos(\omega t + u), \tag{A1}$$

where h_n is the equilibrium potential amplitude of the *n*th constituent, consisting of a constant value h_{on} multiplied by the nodal factor f_n. The variable ω denotes the frequency of this constituent, a constant value usually in cycles per hour. The nodal factor u modulates the phase of this constituent. Both f and u are functions of time but constant for all oceans, and are generally different for each constituent.

[48] Tables of f and u are presented by *Schureman* [1940] for the years 1850 to 1999, and were used for much of the 20th century for all tidal predictions using tidal predicting machines. Modern tidal analyses and prediction software for computers includes the f and u factors implicitly. For example, the most recent versions of the Foreman tidal programs update the values of f and u at monthly intervals. These corrections do not require user intervention, and indeed, many tidal analysts are unaware of them. Interannual variability of tidal current speeds is determined by the f factor, whose average in time is zero by definition. For the period 1850 to 2050 f varies from a low of 0.88 to a high of 1.11 for the principal diurnal constituent K_1, and from 0.95

Table A1. Values of the Constant and Maximum Values of the Variable h_{on} of Nine Constituents in Each Tidal Band, Based on Parameters Defined in the *Foreman* [1977] Tidal Analysis Package and Provided by D. Lee (Personal Communication, 2001)[a]

Diurnal Constit.	Freq. ω_n c/hour *c/day*	Equil. Ampl. h_o, m	Max. f 1850–2050	Semidiurnal Constit.	Freq. ω_n c/hour *c/day*	Equil. Ampl. h_o, m	Max. f 1850–2050
K_1	0.04178 *1.003*	0.223	1.113	M_2	0.08051 *1.932*	0.731	1.038
O_1	0.03873 *0.930*	0.148	1.191	S_2	0.08333 *2.000*	0.352	1.002
P_1	0.04155 *0.997*	0.073	1.014	N_2	0.07900 *1.896*	0.137	1.042
Q_1	0.03722 *0.893*	0.027	1.224	K_2	0.08356 *2.005*	0.099	1.322
NO_1	0.04027 *0.966*	0.013	1.592	NU_2	0.07920 *1.901*	0.026	1.046
J_1	0.04330 *1.039*	0.013	1.296	L_2	0.08202 *1.968*	0.022	1.331
OO_1	0.04483 *1.076*	0.008	1.949	MU_2	0.07769*1.865*	0.022	1.054
SIG_1	0.03591 *0.862*	0.004	1.198	T_2	0.08322 *1.997*	0.021	1.000
PI_1	0.04144 *0.995*	0.004	1.008	$2N_2$	0.07749 *1.860*	0.018	1.154

[a]These constituents arise from variations in lunar and solar tidal strength and phase due to changes in the Earth and lunar orbits.

to 1.05 for M_2. Upper ranges for other constituents are presented in Table A1. The range of f for the largest diurnal constituents is generally large, and in phase across the diurnal band, whereas the variability in the semidiurnal band is small in the largest constituents, and of opposite phase through this band. Therefore the relative nodal modulation is clearly larger in the diurnal band.

[49] These interannual variations in tidal signals cause variations in tidal currents over the same periods. However, the tidal current of the nth constituent is defined as the rate of change of height with time,

$$v_n = \mathrm{d}h_n/\mathrm{dt} = -\omega_n f_n h_{on} \sin(\omega_n t + u_n). \quad \text{(A2)}$$

Therefore equilibrium current speed of a tidal constituent is the product of the frequency of the constituent ω_n multiplied by the height $f_n h_{on}$. This feature boosts the magnitude of semidiurnal currents relative to diurnal.

[50] We have computed a time series of speed cubed for the largest nine constituents in each band for the period 1850 to 2050, using the formula $(v_n)^3 = (\omega_n f_n h_{on})^3$, with values of f_n computed at mid-year, based on factors listed in Table A1. The nine speeds in each band were added and plotted in Figure A1. This figure shows distinct differences between the diurnal and semidiurnal bands. Over the 200 years the diurnal band follows a reasonably regular cycle, whereas the semidiurnal signal, although generally out of phase and comparable in amplitude to the diurnal, also has other components to the signal. Its peaks are sharper and at least three separate signals contribute to the overall effect. Both the perigean (8.85 years) and nodal (18.6 years) effects contribute to the semidiurnal band. If semidiurnal tidal currents followed an equilibrium tide throughout the oceans, then one could expect to see a minimum in semidiurnal mixing peaks in the years near 1970, and maxima near mid-nineteenth and twenty-first centuries due to interactions of the perigean and nodal cycles.

[51] However, local conditions alter the relative behaviour of tidal currents constituents, boosting some and reducing others depending on local resonance and amphidrome configurations. In shallow regions of strong tidal mixing and dissipation the tides themselves may be altered by the changes in dissipation. *Ku et al.* [1985] examine the tidal heights at Saint John in the Bay of Fundy, and reported a nodal modulation in M_2 height of 2.3% rather than the equilibrium value of 3.7%. They attribute the decreased value to attenuation of M_2 by quadratic bottom friction. *Godin* [1994] found modulation in Saint John M_2 of between 2.3% and 2.4% over a discontinuous interval of 77 years.

[52] A second effect attributed to quadratic friction is an additional decrease in the modulation of minor constituents due to the M_2 current dominating the friction. Quoting from *Godin* [1994] "When quadratic friction is applied to a pair of harmonic components, the larger component will be less

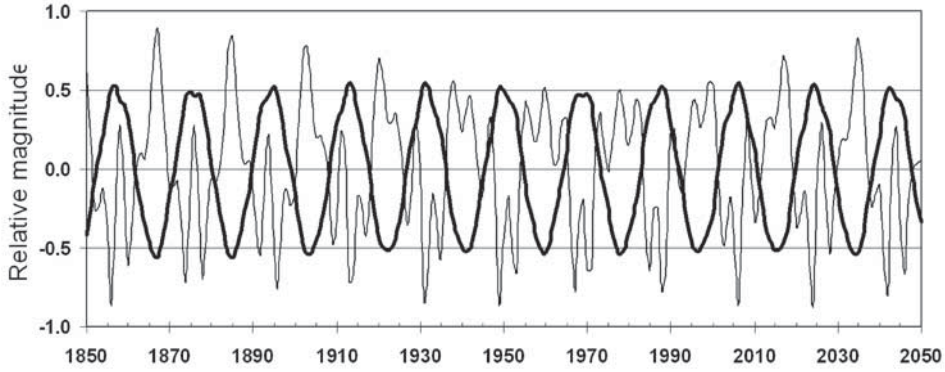

Figure A1. The sum of constituent speed cubed for each of the diurnal (thick line) and semidiurnal (thin line) tidal bands is plotted above, for the period 1850 to 2050. Nine constituents contributed to each band.

damped than the minor one. So if M_2 is larger, S_2 is damped more effectively."

[53] A third effect is the dominance of some shallow water constituents over minor astronomical constituents. For example, *Godin* [1994] notes that the modulation of L_2 at Saint John is due to the modulation of the shallow water tide $2MN_2$, which has the same frequency as L_2. The astronomical L2 has contributions from both second and third order tidal potential terms, and exhibits a 4.5-year periodicity that is not evident in the modulation of $2MN_2$.

[54] Therefore modulation of minor semidiurnal constituents is suppressed by those of the major constituent, usually M_2, in regions of very strong mixing and dissipation. This causes the M_2 modulation to dominate in the semidiurnal band, but has smaller effect in the diurnal band where the major constituents have large, in-phase, modulation.

[55] Therefore, diurnal influences on nodal modulation may be somewhat stronger, and also more coherent over a wider region. In areas of the ocean where diurnal tides are relatively strong, one expects interannual tidal effects to be dominant at the 18.6-year period of the lunar nodal cycle. In spatial extent, diurnal forcing is strongest at mid-latitudes and one can expect variations in sea surface temperature to be evident there. Where semidiurnal tides are relatively strong, it is expected that M_2 modulation will dominate over modulation due to other semidiurnal constituents. The M_2 modulation is 180 degrees out of phase with diurnal modulation.

[56] Astronomical tidal frequencies are known to at least six significant figures. The nodal tidal signals, being essentially line spectra, will emerge from a broadband meteorological signal if a long observational time series is available for spectral analyses.

[57] **Acknowledgments.** Daily surface air temperature records for all climate stations in Canada were obtained from the Meteorological Service of Canada (http://www.msc-smc.ec.gc.ca/climate). Monthly average sea surface temperature and salinity records since the early part of the 20th century are maintained by the staff of Ocean Sciences Division (Institute of Ocean Sciences) of Fisheries and Oceans Canada, and can obtained from (http://www.pac.dfo-mpo.gc.ca/sci/pages/lighthousedata.htm). Ocean current measurements are archived by the Canadian Hydrographic Service at the Institute of Ocean Sciences. Records of daily SST at Scripps Pier (La Jolla, California) and at other sites along the coastal U.S. mainland are maintained and made available by the Shore Station Program of Scripps Institution of Oceanography, UCSD. The NOAA Extended Reconstructed SST data are made available by the NOAA-CIRES ESRL/PSD Climate Diagnostics Branch, Boulder, Colorado, United States, from their website at http://www.cdc.noaa.gov/. The multivariate ENSO index is courtesy of http://www.cdc.noaa.gov/people/klaus.wolter/MEI/mei.html. The Sitka air temperature data are courtesy of Thomas Royer, Old Dominion University.

References

Barnston, A. G., and R. E. Livezey (1987), Classification, seasonality and persistence of low-frequency atmospheric circulation patterns, *Mon. Weather Rev.*, *115*, 1083–1126.

Bond, N. A., J. E. Overland, M. Spillane, and P. Stabeno (2003), Recent shifts in the state of the North Pacific, *Geophys. Res. Lett.*, *30*(23), 2183, doi:10.1029/2003GL018597.

Cerveny, R. S., and J. A. Schaffer (2001), The moon and El Niño, *Geophys. Res. Lett.*, *28*, 25–28.

Chao, Y., M. Ghil, and C. McWilliams (2000), Pacific interdecadal variability in this century's sea surface temperatures, *Geophys. Res. Lett.*, *27*, 2261–2264.

Chavez, F. P., C. A. Collins, A. Huyer, and D. L. Mackas (Eds.) (2002), Observations of the 1997–98 El Niño along the west coast of North America, *Prog. Oceanogr.*, *54*, 511 pp.

Crawford, W. R. (1984), Energy flux and generation of diurnal shelf waves along Vancouver Island, *J. Phys. Oceanogr.*, *14*, 1600–1607.

Crawford, W. R. (1991), Tidal mixing and nutrient flux in the waters of southwest British Columbia, in *Tidal Hydrodynamics*, edited by B. Parker, chap. 44, pp. 855–869, John Wiley, Hoboken, N. J.

Crawford, W. R., and R. E. Thomson (1984), Diurnal period continental shelf waves along Vancouver Island: A comparison of observations with theoretical models, *J. Phys. Oceanogr.*, *14*, 1629–1646.

Currie, R. G. (1996), Variance contribution of luni-solar (M_n) and solar cycle (S_c) signals to climate data, *Int. J. Climatol.*, *16*, 1343–1364.

da Silva, R. R., and R. Avissar (2005), The impacts of the luni-solar oscillation on the Arctic oscillation, *Geophys. Res. Lett.*, *32*, L22703, doi:10.1029/2005GL023418.

DFO (2005), 2004 Pacific region state of the ocean, *DFO Sci. Ocean Status Rep. 2004*, 61 pp.

Doodson, A. T., and H. D. Warburg (1941), *Admiralty Manual of Tides*, 270 pp., Hydrogr. Dep., UK.

Egbert, G. D., and S. Y. Erofeeva (2002), Efficient inverse modeling of barotropic ocean tides, *J. Atmos. Oceanic Technol.*, *19*, 183–204.

Emery, W. J., and K. Hamilton (1985), Atmospheric forcing of interannual variability in the northeast Pacific Ocean: Connections with El Niño, *J. Geophys. Res.*, *90*(C1), 857–868.

Ffield, A., and A. L. Gordon (1996), Tidal mixing signatures in the Indonesian seas, *J. Phys. Oceanogr.*, *26*, 1924–1937.

Foreman, M. G. G. (1977), Manual for tidal heights analysis and prediction, *Pac. Mar. Sci. Rep. 77-10*, 101 pp., Inst. of Ocean Sci., Fish. and Oceans Can., Sidney, B. C., Canada.

Foreman, M. G. G. (1978), Manual for tidal currents analysis and prediction, *Pac. Mar. Sci. Rep. 78-6*, 70 pp., Inst. of Ocean Sci., Fish. and Oceans Can., Sidney, B. C., Can.

Foreman, M. G. G., W. R. Crawford, J. Y. Cherniawsky, R. F. Henry, and M. Tarbotton (2000), A high-resolution assimilating tidal model for the Northeast Pacific Ocean, *J. Geophys. Res.*, *105*, 28,629–28,652.

Foreman, M. G. G., P. F. Cummins, J. Y. Cherniawsky, and P. Stabeno (2006), Tidal energy in the Bering Sea, *J. Mar. Res.*, in press.

Fritts, H. C. (1991), *Reconstructing Large-Scale Climatic Patterns From Tree-Ring Data*, 286 pp., Univ. of Ariz. Press, Tucson.

Garrett, C. (2003), Internal tides and ocean mixing, *Science*, *301*, 1858.

Godin, G. (1994), Confirmation of the trends expected to be present in the tide of the Bay of Fundy, *Int. Hydrogr. Rev.*, *LXXI*(2), 103–117.

Ku, L.-F., D. A. Greenberg, C. J. R. Garrett, and F. W. Dobson (1985), Nodal modulation of the lunar semidiurnal tide in the Bay of Fundy and Gulf of Maine, *Science*, *230*, 69–71.

Lluch-Cota, D. B., W. S. Wooster, and S. R. Hare (2001), Sea surface temperature varability in coastal areas of the northeastern Pacific related to El Nino-Southern Oscillation and Pacific Decadal Oscillation, *Geophys. Res. Lett.*, *28*, 2029–2032.

Loder, J. W., and C. Garrett (1978), The 18.6-year cycle of sea surface temperature in shallow seas due to tidal mixing, *J. Geophys. Res.*, *83*, 1967–1970.

Mantua, N. J., and S. R. Hare (2002), The Pacific Decadal Oscillation, *J. Oceanogr.*, *58*(1), 35–44.

Mantua, N., S. R. Hare, Z. Zhang, J. M. Wallace, and R. C. Francis (1997), A Pacific decadal oscillation with impacts on salmon production, *Bull. Am. Meteorol. Soc.*, *78*, 1069–1079.

McGowan, J. A., D. R. Cayan, and C. E. Dorman (1998), Climate-ocean variability and ecosystem response in the northeast Pacific, *Science*, *281*, 210–217.

McKinnell, S. M., H. J. Freeland, and S. D. Groulx (1999), Assessing the northern diversion of sockeye salmon returning to the Fraser River, BC, *Fish. Oceanogr.*, *8*, 104–114.

Ono, T., T. Midorikawa, Y. W. Watanabe, K. Tadokoro, and T. Saino (2001), Temporal increases of phosphate and apparent oxygen utilization in the subsurface waters of western subarctic Pacific from 1968 to 1998, *Geophys. Res. Lett.*, *28*(17), 3285–3288.

Osafune, S., and I. Yasuda (2006), Bidecadal variability in the intermediate waters of the northwestern subarctic Pacific and the Okhotsk Sea in relation to the 18.6-year period nodal tidal cycle, *J. Geophys. Res.*, *111*, C05007, doi:10.1029/2005JC003277.

Qu, T., Y. Du, J. Strachan, G. Meyers, and J. Slingo (2005), Sea surface temperature and its variability in the Indonesian region, *Oceanography*, *18*, 50–61.

Roden, G. I. (1961), On nonseasonal temperature and salinity variations along the west coast of the United States and Canada, annual report, CalCOFI, San Diego, Calif.

Roden, G. I. (1989), Analysis and intepretation of long-term climatic variability along the west coast of North America, in *Aspects of Climate Variability in the Pacific and the Western Americas*, *Geophys. Monogr. Ser.*, vol. 55, edited by D. H. Peterson, pp. 93–111, AGU, Washington, D. C.

Rogachev, K. A., E. C. Carmack, A. S. Salomatin, and M. G. Alexanina (2001), Lunar fortnightly modulation of tidal mixing near Kashevarov

Bank, Sea of Okhotsk, and its impacts on biota and sea ice, *Prog. Oceanogr.*, *49*, 373–390.

Royal, L. A., and J. P. Tully (1961), Relationships of variable oceanographic factors to migration and survival of Fraser River salmon, *CALCOFI Rep.*, *8*, 65–68.

Royer, T. (1993), High-latitude oceanic variability associated with the 18.6-year nodal tide, *J. Geophys. Res.*, *98*, 4639–4644.

Schureman, P. (1940), *Manual of Harmonic Analysis and Prediction of Tides*, *Spec. Publ. 98*, 317 pp., U.S. Dep. of Commer., U.S. Govt. Print. Off., Washington, D. C.

Schwing, F. B., T. Murphree, and P. M. Green (2002), The Northern Oscillation Index (NOI): a new climate index for the northeast Pacific, *Prog. Oceanogr.*, *53*, 115–139.

Simpson, J. H., and J. R. Hunter (1974), Fronts in the Irish Sea, *Nature*, *250*, 404–406.

Strub, P. T., and C. James (2002), The 1997–1998 El Niño signal along the southeast and northeast Pacific boundaries—an altimetric view, *Prog. Oceanogr.*, *54*, 439–458.

Subbotina, M. M., R. E. Thomson, and A. B. Rabinovich (2001), Spectral characteristics of sea level variability along the west coast of North America during the 1982–83 and 1997–98 El Niño events, *Prog. Oceanogr.*, *49*, 353–372.

Tabata, S. (1985), El Niño effects along and off the coast of Canada during 1982–83, in *El Niño North: El Niño Effects in the Eastern Subarctic Pacific Ocean*, edited by W. S. Wooster and D. L. Fluharty, pp. 85–96, Univ. of Wash., Seattle.

Tabata, S. (1989), Trends and long-term variability of ocean properties at Ocean Station P in the northeast Pacific Ocean, in *Aspects of Climate Variability in the Pacific and Western Americas*, *Geophys. Monogr. Ser.*, vol. 55, edited by D. H. Peterson, pp. 113–132, AGU, Washington, D. C.

Thejll, P. A. (2001), Decadal power in land air-temperatures: Is it statistically significant?, *J. Geophys. Res.*, *106*(D23), 31,693–31,702.

Trenberth, K. E., and J. W. Hurrell (1994), Decadal atmosphere-ocean variations in the Pacific, *Clim. Dyn.*, *9*, 303–319.

Tully, J. P. (1937), Gradient currents, *Pac. Prog. Rep. 32*, pp. 13–14, Fish. Res. Board, Ottawa, Ont., Canada.

Tully, J. P., A. J. Dodimead, and S. Tabata (1960), An anomalous increase of temperature in the ocean off the Pacific coast of Canada through 1957 to 1958, *J. Fish. Res. Board Can.*, *17*, 61–80.

Ware, D. W., and R. E. Thomson (2000), Interannual to multidecadal climate variations in the northeast Pacific, *J. Clim.*, *13*, 3209–3220.

Watanabe, Y. W., M. Wakita, N. Maeda, T. Ono, and T. Gamo (2003), Synchronous bidecadal periodic changes of oxygen, phosphate and temperature between the Japan Sea and the North Pacific intermediate water, *Geophys. Res. Lett.*, *30*(24), 2273, doi:10.1029/2003GL018338.

Wolter, K., and M. S. Timlin (1998), Measuring the strength of ENSO – how does 1997/98 rank?, *Weather*, *53*, 315–324.

Wooster, W. S., and D. L. Fluharty (Eds.) (1985), *El Niño North*, 312 pp., Univ. of Wash. Sea Grant Program, Seattle.

Yasuda, I., S. Osafune, and H. Tatebe (2006), Possible explanation linking 18.6-year period nodal tidal cycle with bi-decadal variations of ocean and climate in the North Pacific, *Geophys. Res. Lett.*, *33*, L08606, doi:10.1029/2005GL025237.

W. R. Crawford, Fisheries and Oceans Canada, Institute of Ocean Sciences, P.O. Box 6000, 9860 W. Saanich Road, Sidney, BC, Canada V8L 4B2.

S. M. McKinnell, North Pacific Marine Science Organization, c/o Institute of Ocean Sciences, P.O. Box 6000, 9860 W. Saanich Road, Sidney, BC, Canada V8L 4B2. (mckinnell@pices.int)